

*This thesis is
dedicated
to
My Daughter*

Statement by author

This dissertation has been presented to meet the partial requirements for the attainment of an advanced degree at the University of North Bengal (NBU) and has been deposited in the library for lending under the regulations of the NBU. Brief excerpts from this dissertation may be used without special permission, provided proper acknowledgment of the source is made. Requests for permission to reproduce or quote extensively from this manuscript, in whole or in part, may be granted by the authorized personnel of NBU if deemed beneficial for academic purposes. Otherwise, permission must be sought from the author.

Madan Rajbanshi
Madan Rajbanshi

Declaration

I hereby declare that his thesis entitled "**Understanding the Target Analyte Interaction for the Design and Development of Efficient Optical Sensor: A Combined Photophysical and Theoretical Analysis**" embodies my original research work, conducted under the supervision of Dr. Sudhir Kumar Das, at the Department of Chemistry, University of North Bengal.

The work presented in this thesis results from my independent investigation and reflects my efforts and understanding of the subject matter. All the data, results, and conclusions presented in this document are based on genuine research findings and have not been previously submitted for any other degree or qualification at this or any other institution.

I affirm that the content of this thesis is the result of my research work and is presented with the utmost honesty and integrity.

Madan Rajbanshi

MADAN RAJBANSHI

Department of Chemistry

University of North Bengal

Darjeeling-734013

West Bengal, India

Date: 08-04-2024

UNIVERSITY OF NORTH BENGAL

Dr. Sudhir Kumar Das, Ph. D
Assistant Professor
Department of Chemistry
North Bengal University
Darjeeling, 734013
India



समानो मन्त्रः समितिः समानी

Email: sudhirkumardas@nbu.ac.in

Mobile: 91-8016884965

Accredited by NAAC with Grade B⁺⁺

Certificate

It is certified that the work contained in the thesis titled "**Understanding the Target Analyte Interaction for the Design and Development of Efficient Optical Sensor: A Combined Photophysical and Theoretical Analysis,**" by "**MADAN RAJBANSHI,**" has been carried out under my supervision and that this work has not been submitted elsewhere for a degree.


08-04-2024
Dr. Sudhir Kumar Das

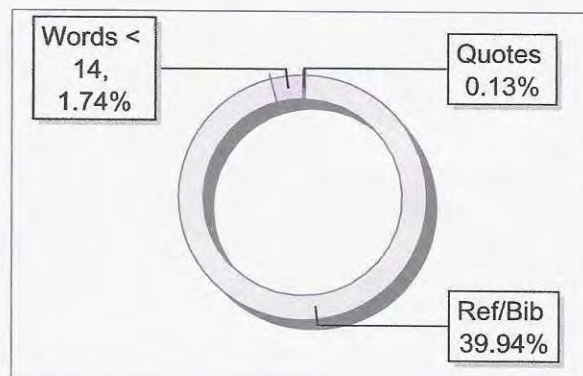
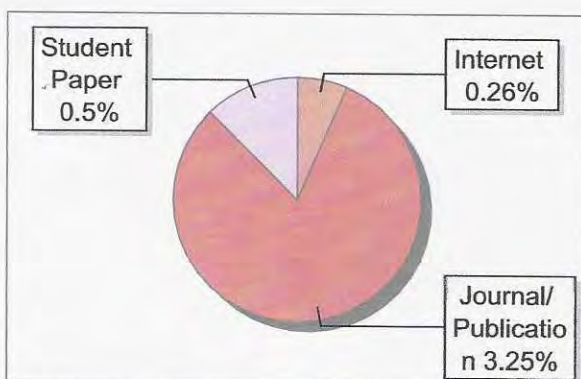
Dr. Sudhir Kumar Das
Assistant Professor
Department of Chemistry
University of North Bengal
Darjeeling - 734013, India
Department of Chemistry
North Bengal University
Darjeeling, 734013

Submission Information

Author Name Madan Rajbanshi
Title Understanding the Target Analyte Interaction for the Design and Development of Efficient Optical Sensor: A Combined Photophysical and Theoretical Analysis
Paper/Submission ID 1454083
Submitted by nbuplg@nbu.ac.in
Submission Date 2024-02-21 14:22:24
Total Pages 112
Document type Thesis

Result Information

Similarity 4 %



Exclude Information

Quotes Excluded
References/Bibliography Excluded
Sources: Less than 14 Words % Not Excluded
Excluded Source 2 %
Excluded Phrases Not Excluded

Database Selection

Language English
Student Papers Yes
Journals & publishers Yes
Internet or Web Yes
Institution Repository Yes

Dr. Sudhir Kumar Das
06.04.24
Assistant Professor
Department of Chemistry
University of North Bengal
Darjeeling - 734013, India

Unique QR Code use to View/Download/Share Pdf File

Madan Rajbanshi



Preface

I set off my journey for research work regarding to Doctor of Philosophy (Ph.D.) degree under the supervision of Dr. Sudhir kumar Das in 2019 in the Department of Chemistry, University of North Bengal (NBU). The thesis, entitled “**Understanding the Target Analyte Interaction for the Design and Development of Efficient Optical Sensor: A Combined Photophysical and Theoretical Analysis**” represents the termination of the journey to obtain the desired degree and the outcomes of several years of diligent study and investigation are gathered in this thesis. The date of registration for my Ph.D. program at NBU is 02/01/2019, vide letter no. Ph.D/Chem. (1722)/623/R-2023.

Here some optical sensors have been designed and developed and the whole thesis is an attempt to understand the interaction between the target analyte and sensor by measuring the change of some photophysical properties experimentally in the spectroscopic method. Further, these experimental results obtained from photophysical analysis have been correlated with theoretical calculations applying DFT.

Acknowledgment

I am incredibly grateful to my supervisor, **Dr. Sudhir Kumar Das**, for his important advice and mentorship throughout my research work. His vast knowledge and enthusiasm for science have motivated me to work well in the laboratory. I want to convey my sincere thanks to **Prof. Bhaskar Biswas**, Head of the Department of Chemistry, University of North Bengal for giving necessary resources, advice, and administrative help during my research. I am thankful to all my lab mates, especially **Manas Mahato, Ziaur Rahaman, Pallobi Sarkar, Tuhina Sultana, Najmin Tohora, Sabbir Ahamed, and Jyoti Chourasia**. I am also thankful to all other scholars of the department for their constant support and companionship. I want to convey thanks to my family members for their constant support during this challenging endeavor. I am also grateful to my friends **Somnath Karmakar, Litan Bhakta, and Kishalay Sharma** who helped, and my brother, **Bappa Debnath** supported me in various matters related to Research work. Without the collective assistance/ help and encouragement of these people and organizations, this thesis would not have been feasible.

Madan Rajbanshi

Mr. Madan Rajbanshi

Research Scholar

Department of Chemistry

University of North Bengal

Darjeeling-734013, INDIA

List of figures

Figures		Page No
Figure 1.1.	Schematic presentation of chemosensor.	5
Figure 1.2.	Schematic diagram of the PET process.	9
Figure 1.3.	(a) Diagram for recognition of cation (bounded to donor site) utilizing fluorescent ICT optical chemosensors. (b) Diagram for cation recognition (bounded to acceptor site) utilizing fluorescent ICT optical chemosensors.	10
Figure 1.4.	Schematic diagram showing paramagnetic fluorescence quenching.	10
Figure 1.5.	Diagram of the FRET approach.	11
Figure 1.6.	Diagram for the photophysical cycle of ESIPT.	12
Figure 2.1.	¹ H NMR spectra of prepared HBAN in DMSO- <i>d</i> ₆ .	23
Figure 2.2.	¹³ C NMR spectrum of as-prepared of HBAN .	23
Figure 2.3.	The IR spectrum of prepared HBAN .	24
Figure 2.4.	High-resolution mass spectrum of prepared HBAN .	24
Figure 2.5.	(a) Spectrophotometric absorption titration spectra of probe- HBAN with Al ³⁺ (0 equiv. to 3 equiv.) ions. (Inset: visual color changes of free probe- HBAN due to the introduction of Al ³⁺ ions). (b) Change of absorbance values of HBAN solution at the wavelength 480 nm and 380 nm due to the introduction of Al ³⁺ (0 to 3 equiv.) ions and (c) Ratiometric calibration plot of [Al ³⁺] vs. log(A ₄₈₀ /A ₃₈₀).	25
Figure 2.6.	(a) Fluorescence titration spectra of HBAN up to the introduction of 3 equiv. of Al ³⁺ ions. (b) Linear calibration curve of the photoluminescence intensity at 540 nm vs. [Al ³⁺] to calculate the limit of detection (LOD) employing our probe HBAN . (c) Corresponding CIE diagram for free probe- HBAN and HBAN -Al ³⁺ complex. (d) Photoluminescence response time of HBAN for Al ³⁺ ions detection. (e) Fluorescence intensity for the reverse titration at a particular concentration of Al ³⁺ ions with the variation of concentration of HBAN .	27
Figure 2.7.	Time-resolved fluorescence decay profile of HBAN in DMF. The excitation and monitored wavelength are 375 nm and 540 nm, respectively.	28
Figure 2.8.	(a) Metal ion selectivity test of HBAN (2.34 × 10 ⁻⁵ M) upon	31

	introduction of various metal ions (7.91×10^{-5} M). (b) Colorimetric change HBAN solution due to the introduction of metal ions under a 365 nm UV lamp irradiation.	
Figure 2.9.	Change of fluorescence intensity of the solution of HBAN in the presence of (a) 3 equiv. of Al^{3+} ions upon the addition of 3 equiv. of other competing metal ions and (b) 3 equiv. of Al^{3+} ions upon the addition of 3 equiv. of various competing anions.	32
Figure 2.10.	(a) Job's plot for the finding of stoichiometric ratio of HBAN with Al^{3+} ions. (b) Job's plot for the binding of HBAN with Al^{3+} from UV-visible spectral analysis. (c) Benesi-Hildebrand plot for the determination of association constant of HBAN (2.34×10^{-5} M) with Al^{3+} (0 to 3 Equiv.).	32
Figure 2.11.	^1H NMR titration spectra of HBAN due to the introduction of Al^{3+} ions in $\text{DMSO-}d_6$.	33
Figure 2.12.	FT-IR spectra of HBAN and Al^{3+} ions chelated HBAN complex.	33
Figure 2.13.	Optimized structure of (a) HBAN and (b) Al^{3+} ions chelated HBAN complex at the level of CAM-B3LYP/6-31+g** and B3LYP/6-31+g** theory, respectively.	35
Figure 2.14.	Pictorial representation of FMOs and corresponding transition of (a) HBAN and (b) Al^{3+} ions chelated HBAN complex at the level of CAM-B3LYP/6-31+g** and B3LYP/6-31+g** theory respectively.	35
Figure 2.15.	Theoretically, the predicted UV-visible absorption band of the free- HBAN molecule and Al^{3+} ions chelated HBAN complex.	36
Figure 2.16.	(a) Fluorescence titration spectra of Al^{3+} chelated HBAN complex due to the stepwise addition of PA and (b) Changes of fluorescence intensity of Al^{3+} chelated HBAN complex due to the addition of 5equiv. various NACs, (c) Fluorescence intensity changes of the Al^{3+} ions chelated HBAN complex solution and four equivalent of PA upon addition of 5 eq. of other competing NACs.	37
Figure 2.17.	(a) Stern-Volmer plot of the quenching of HBAN on interaction with the PA. (b) Linear plot for the calculation of dynamic quenching constant.	38
Figure 2.18.	Calibration curve of [PA] vs. fluorescence intensity of Al^{3+} ions chelated HBAN complex for calculating the LOD.	38
Figure 2.19.	Demonstration of formation of INHIBIT logic gate (a) The truth	40

table is used to build the INHIBIT logic gate. **(b)** Graphical representation of the built INHIBIT logic gate. **(c)** Changes of fluorescence intensity at 540 nm in the presence of Al^{3+} ions and PA, respectively, as optical outputs. **(d)** Display of color changes visible to the naked eye when exposed to 365 nm light as optical outputs.

Figure 2.20.	(a) Fluorescence color variations of HBAN (3mM) loaded filter paper in the presence of various metal ions (1 mM) while illuminated by a portable 365 nm UV lamp. (b) Pictorial representation of HBAN -coated paper strips-based test kit to detect environmental water samples. (c) Photograph of PA detection by HBAN -coated paper strips-based test kit method.	41
Figure 3.1.	^1H NMR spectra of prepared Z1 in DMSO-d_6 .	52
Figure 3.2.	^{13}C NMR spectra of our prepared MATC in DMSO-d_6 .	52
Figure 3.3.	The IR spectrum of prepared Z1 .	53
Figure 3.4.	High-resolution Mass Spectrum of prepared Z1 .	53
Figure 3.5.	(a) UV-visible absorption spectral change of Z1 due to the addition of AcOH in ACN and (b) the change of absorbance values with the addition of acid concentration, respectively. (c) UV-visible absorption spectral changes of Z1 due to the addition of TFA and (d) the corresponding change in optical density values with the addition of acid.	54-55
Figure 3.6.	Energy profile diagram for Z1 , Z1+H⁺(NH) , and Z1+H⁺(OH) systems.	57
Figure 3.7.	Frontier molecular orbital for Z1 and Z1+H⁺(OH) systems.	57
Figure 3.8.	(a) Experimental UV-visible absorption spectra of Z1 and Z1+H⁺ systems upon protonation (upper panel) and theoretical Z1 , Z1+H⁺(NH) , and Z1+H⁺(OH) systems (lower panel). (b) Frontier molecular orbital for Z1 and Z1+H⁺(NH) systems.	57
Figure 3.9.	Visual color changes of paper strips of Z1 in the presence of TFA (a) and its reversibility (b) upon the addition of different concentrations of TEA.	58
Figure 3.10.	Visual color of paper test strips of (a) probe Z1 ($1 \times 10^{-3}\text{M}$), (b) upon passing TFA vapor ($1 \times 10^{-4}\text{ M}$ - $4 \times 10^{-4}\text{ M}$), and (c) its reversibility in the presence of ($1 \times 10^{-4}\text{ M}$ - $4 \times 10^{-4}\text{ M}$) TEA.	59

Figure 3.11.	Plot of pH vs log ([In-] / [HIn]) of Z1 in acetonitrile.	61
Figure 3.12.	The absorption spectrum of Z1 during titration by TFA in acetonitrile at 25°C.	61
Figure 3.13.	The absorption spectrum of Z1 during titration by SA in acetonitrile at 25°C.	61
Figure 3.14.	Absorption spectra of Z1 during titration by MeSO ₃ H in acetonitrile at 25°C.	62
Figure 3.15.	Absorption spectra of Z1 during titration by oxalic acid in acetonitrile at 25°C.	62
Figure 3.16.	Absorption spectra of Z1 during titration by formic acid in acetonitrile at 25°C.	62
Figure 3.17.	(a, b) Reversible UV-visible spectra of Z1 +AcOH and Z1 +TFA with TEA respectively.	64
Figure 3.18.	Color changes upon the addition of TEA to the solution containing Z1 +H ⁺ .	64
Figure 3.19.	A schematic illustration of a complementary output INH and IMP circuit.	65
Figure 4.1.	¹ H NMR spectra of prepared BEN in DMSO -d ₆ .	72
Figure 4.2.	¹³ C NMR spectrum of as-prepared BEN .	72
Figure 4.3.	The IR spectrum of prepared BEN .	73
Figure 4.4.	High-resolution Mass Spectrum of prepared BEN .	73
Figure 4.5.	(a) UV-visible spectrophotometric titration spectra of BEN solution (2.34 × 10 ⁻⁵ M) due to the gradual addition of F ⁻ ions (0 equiv. to 1.83 equiv.), (Inset: Colorimetric change of BEN solution due to introducing F ⁻ ions). (b) Variation in absorbance values of BEN solution at 520 nm with the increase in the concentration of F ⁻ ions (0 – 1.83 equiv.).(Inset: Change in UV-visible absorption spectra of BEN solution from 434 nm to 675 nm with increased concentration of F ⁻ ions (0 – 1.83 equiv.).	74
Figure 4.6.	(a) UV-visible absorption titration spectra of BEN solution by gradually adding CN ⁻ ions (0 equiv. to 1.83 equiv.). (b) UV-visible absorption of BEN solution by gradually adding AcO ⁻ ion (0 equiv. to 1.83 equiv.).	74
Figure 4.7.	Response time of BEN toward three anions in colorimetric detection.	75
Figure 4.8.	(a) Change of UV-visible absorption spectral features of BEN	76

solution with 1.83equiv.of different anions. **(b)** Bar diagram demonstrating the change in absorbance values at 520 nm of **BEN** solution on addition of various anions (1.83 equiv.). **(c)** Photograph of anion selectivity experiment of **BEN** solution with 1.83 equiv. of different anions in daylight.

- Figure 4.9.** **(a)** UV-visible spectral behavior of **BEN** solution under the anionic crowding situations (1.83 equiv.) in the presence of each of F^- , CN^- , and AcO^- anions (1.83 equiv.). **(b)** Image of glass vials containing **BEN** solution mixed with various anions (1.83 equiv.) in the presence of each of F^- , CN^- , and AcO^- anions (1.83 equiv.). 77
- Figure 4.10.** Job's plot for determination of stoichiometric ratio between **(a)** **BEN** and F^- **(b)** **BEN** and CN^- and **(c)** **BEN** and AcO^- from UV-visible absorption data. 78
- Figure 4.11.** Benesi-Hildebrand plot to estimate the binding constant between **(a)** **BEN** (2.344×10^{-5} M) and F^- (0 to 1.83 Equiv.) in F^- -**BEN** adduct. **(b)** **BEN** (2.344×10^{-5} M) and CN^- (0 to 1.83 Equiv.) in CN^- -**BEN** adduct and **(c)** **BEN** (2.344×10^{-5} M) and AcO^- (0 to 1.83 Equiv.) in AcO^- -**BEN** adduct. 78
- Figure 4.12.** The plot of **(a)** absorbance vs. $[F^-]$ **(b)** absorbance vs. $[CN^-]$ and **(c)** absorbance vs. $[AcO^-]$ at 520 nm for estimation of the detection limit of **BEN** for the detection of F^- , CN^- and AcO^- in DMF solvent respectively. 78
- Figure 4.13.** 1H NMR titration Spectra of **BEN** with different quantities of F^- ions in $DMSO-d_6$. 79
- Figure 4.14.** 1H NMR titration Spectra of **BEN** with different quantities of CN^- ions in $DMSO-d_6$ solvent. 80
- Figure 4.15.** 1H NMR titration Spectra of **BEN** with different quantities of AcO^- ions in $DMSO-d_6$ solvent. 80
- Figure 4.16.** **(a)** Spectral changes of UV-visible absorption spectra of **BEN-F** adduct in DMF solution by stepwise adding of HSO_4^- (20 μM) ions. **(b)** Reversibility of absorbance and color of **BEN** solution at 520 nm for five cycles due to the alternative introduction of F^- and HSO_4^- in DMF medium. 81
- Figure 4.17.** **(a)** Absorbance spectra of cation interference in DMF solution. **(b)** and the corresponding bar diagram at 520 nm. 81
- Figure 4.18** **(a)** Image of colorimetric change of filter paper pieces coated with 82

	BEN due to the presence of various anions in daylight. (b) Colorimetric changes of BEN -coated paper strip-based test kit in the spikes of anions in aqueous environment. (c) Photograph on colorimetric changes of BEN -coated ordinary paper in the presence of target anions.	
Figure 4.19.	(a) Truth table for the formation of inhibit molecular logic gate. (b) Pictorial presentation of the constructed gate. (c) Logic gate-related bar diagram of absorbance values at 520 nm of free BEN solution and the addition of other input. (d) Photograph of glass vials containing free BEN solution and due to the addition of other analytes in daylight.	83
Figure 4.20.	(a) Pictorial presentation of the sequential logic circuit of the memory gadget. (b) The truth table of the logic circuit. (c) Pictorial demonstration of the feedback loop presenting reversible logic operation by applying two inputs (Set and Reset) having "Write–Read–Erase–Read" functionalities.	84
Figure 4.21.	Image of the intensity change in RGB color of the BEN solution ($2.34 \times 10^{-5}M$) in different concentrations of (a) F^- (b) CN^- and (c) AcO^- ions.	84
Figure 4.22.	The plot of (a) R/G vs. $[F^-]$ (b) R/G vs. $[CN^-]$ and (c) R/G vs. $[AcO^-]$ for estimation of the LOD of BEN solution for detecting F^- , CN^- and AcO^- ions respectively in DMF solvent.	85
Figure 5.1.	1H NMR spectrum of our prepared probe MATC in $DMSO-d_6$.	92
Figure 5.2.	^{13}C NMR spectra of our prepared MATC in $DMSO-d_6$.	92
Figure 5.3.	The IR spectrum of prepared MATC .	93
Figure 5.4.	High-resolution mass spectra of our synthesized MATC .	93
Figure 5.5.	(a) Normalized UV-visible absorption spectra of coumarin151 and MATC . (b) Changes in absorbance of MATC solution at 402 nm due to a gradual increase in the concentration of DCP (0 – 4.8 equiv.) in the titration. (Inset: Change in absorption spectra of MATC solution in the range from 450 nm to 402 nm due to an increase in the concentration of DCP (0 – 4.8 equiv.) gradually).	94
Figure 5.6.	(a) Spectrophotometric titration spectra of MATC solution (7.8 μM) with stepwise addition of DCP (0 - 4.8 equiv.) in pure ACN. (Inset: Image of vial represents a naked eye color change of MATC solution by DCP at the end of the spectrophotometric	95

- titration). **(b)** Normalized UV-visible absorption spectra coumarin151 and **MATC+DCP**.
- Figure 5.7.** **(a)** Normalized emission spectra of coumarin151 and **MATC**. **(b)** 96
 Normalized absorbance and fluorescence spectra of **MATC**. **(c)**
 Fluorescence titration spectra of **MATC** solution (7.8 μ M) by the
 gradual adding of DCP up to 7.6 equivalents in pure ACN solvent.
 Inset: Image of emission color change of **MATC** solution without
 DCP and with 7.6 equivalents of DCP in the presence of UV-
 irradiation (365nm). **(d)** Variation in fluorescence intensity of
MATC solution at 463 nm due to the gradual increase in the
 concentration of DCP (0 – 7.6 equiv.) in the titration. **(e)**
 Photoluminescence response time of **MATC** for detection of nerve
 agent mimic, DCP.
- Figure 5.8.** **(a)** Bar diagram demonstrating the fluorescence intensity of Blank 97-98
 solution in ACN solvent on adding the exact equivalents of DCP
 and other analytes (7.6 equivalents) at 463 nm. **(b)** The picture of
MATC solution in ACN solvent on the addition of DCP and other
 analytes (7.6 equivalents) under 365 nm UV light irradiation
 where (1) **MATC**, (2) DCP, (3) TEP, (4) T2CP, (5) TMP, (6)
 TIMEP, (7) DMMP, (8) NaH_2PO_4 , (9) Na_2HPO_4 , (10) Na_3PO_4 ,
 (11) DCNP, (12) HCl, (13) TA, (14) TEA, (15) BB, (16) BA, (17)
 MCE, (18) CH_3COOH , (19) POCl_3 , (20) 2CES, (21) 2CPS.
- Figure 5.9.** ^1H NMR titration spectra of **MATC** due to the stepwise 99
 accumulation of DCP in $\text{DMSO}-d_6$.
- Figure 5.10.** Linear calibration curve of the fluorescence intensity of **MATC** 100
 solution vs. concentration of DCP in ACN at 463 nm to estimate
 LOD and LOQ values.
- Figure 5.11.** Image displaying **(a)** selective response of Blank deposited filter 102
 paper strips in the presence of DCP and other analytes solution
 with the exposure of 365 nm UV lamp. **(b)** Colorimetric variation
 in photoluminescence intensity of blank-coated test-kit in
 numerous concentrations (10^{-9} to 10^{-3} M) of DCP solution under
 the movable 365 nm UV light illumination.
- Figure 5.12.** Photograph demonstrating **(a)** selective response of **MATC** in the 103
 dip-stick method in the presence of DCP and other analytes under
 365nm UV light where(1) **MATC**, (2) DCP, (3) DMMP, (4)

T2CP, (5) TMP, (6) TIMEP, (7) TEP, (8) POCl₃, (9) Na₂HPO₄, (10) Na₃PO₄, (11) DCNP, (12) NaH₂PO₄, (13) TA, (14) TEA, (15) HCl, (16) BA, (17) MCE, (18) CH₃COOH, (19) BB, (20) 2CES, (21) 2CPS. **(b)** Change in fluorescence intensity of **MATC** in various concentrations (10^{-9} to 10^{-3} M) of DCP under a 365 nm UV light. **(c)** Photoluminescence response of **MATC** solution in conical flask test **(1)** in the absence and **(2)** presence of DCP vapor under 365 nm UV light radiations.

List of tables

Tables	Page No
Table 2.1. Comparison of the requirements of various Al ³⁺ ions chemosensors	28
Table 2.2. Comparison with the limit of detection of sensing PA by several sensors.	38
Table 3.1. Estimated and average p <i>K</i> _a of several acids in acetonitrile at 25 °C	63
Table 3.2. Truth table for logic function of INHIBIT (INH) and IMPLICATION (IMP) gate.	65
Table 5.1. Comparison table of chemosensors introduced for the detection of nerve agent stimulants in the last few decades with our probe MATC	104

List of appendices

Appendices	Page No.
I: List of publication	112
II: List of seminars/conferences/workshops attended	113